Targeted Mechanical Properties for Optimal Fluid Motion Inside Artificial Bone Substitutes

L.D. Blecha,[1] L. Rakotomanana,[2] F. Razafimahery,[2] A. Terrier,[1] D.P. Pioletti[1]

[1]Laboratory of Biomechanical Orthopedics EPFL-HOSR, 1005 Lausanne, Switzerland, [2]IRMAR, University of Rennes, Rennes, France

Received 18 January 2008; accepted 17 November 2008
Published online 29 January 2009 in Wiley InterScience (www.interscience.wiley.com). DOI 10.1002/jor.20836

ABSTRACT: Our goal was to develop a method to identify the optimal elastic modulus, Poisson's ratio, porosity, and permeability values for a mechanically stressed bone substitute. We hypothesized that a porous bone substitute that favors the transport of nutriments, wastes, biochemical signals, and cells, while keeping the fluid-induced shear stress within a range that stimulates osteoblasts, would likely promote osteointegration. Two optimization criteria were used: (i) the fluid volume exchange between the artificial bone substitute and its environment must be maximal and (ii) the fluid-induced shear stress must be between 0.03 and 3 Pa. Biot's poroelastic theory was used to compute the fluid motion due to mechanical stresses. The impact of the elastic modulus, Poisson's ratio, porosity, and permeability on the fluid motion were determined in general and for three different bone substitute sizes used in high tibial osteotomy. We found that fluid motion was optimized in two independent steps. First, fluid transport was maximized by minimizing the elastic modulus, Poisson's ratio, and porosity. Second, the fluid-induced shear stress could be adjusted by tuning the bone substitute permeability so that it stayed within the favorable range of 0.03 to 3 Pa. Such method provides clear guidelines to bone substitute developers and to orthopedic surgeons for using bone substitute materials according to their mechanical environment. © 2009 Orthopaedic Research Society. Published by Wiley Periodicals, Inc. J Orthop Res 27:1082–1087, 2009

Keywords: bone fluid; scaffold; tissue engineering

Ceramics and polymer porous structures can be produced with controlled pore size, porosity, mechanical resistance, and surface properties.[1–5] Thus, novel artificial bone substitutes can be customized as to their physical properties. The question becomes which material favored best osteointegration in order to shorten the postoperative recovery phase. Much effort has been spent on searching for the optimal bone substitute architecture with regard to degradation rate and osteointegration.[6–12] Empirical studies show that pore interconnectivity must be >50 μm and pore diameter must be >100 μm, although this latter value is still debated.[13,14] No consensus has emerged on optimal permeability, porosity, and bulk stiffness. The need exists, therefore, to develop a synthetic approach to define target mechanical and fluid conductivity properties that likely favor osteointegration.

To develop such an approach, the mechanical environment and the associated fluid motion must be considered. Many physico-chemical and biological phenomena are involved in osteointegration, but fluid motion due to mechanical loading plays a central role in bone substitute osteointegration,[15] bone mechanotransduction,[16,17] and angiogenesis.[18,19] Indeed, the transport of nutriments, wastes, biochemical signals, and cells throughout the substitute stimulates osteoblasts.[20,21] In addition, fluid motion exerts direct mechanical stress on bone cells that can stimulate[22] or damage[23] cells, depending on its magnitude. Shear stress between 0.03 and 3 Pa triggers production of essential proteins by osteoblasts cultured in vitro on two-[24–31] and three-[20,22,32–34] dimensional supports and favors angiogenesis in vivo.[18] Conversely, fluid-induced shear stress >10 Pa compromises cell membrane integrity and function.[35] Thus, a balance between maximal particle transport and optimal fluid-induced shear stress must be achieved to favor bone substitute osteointegration.

Our goal was to identify elastic modulus, Poisson's ratio, porosity, and permeability values that optimize internal fluid motion in a bone substitute subjected to a specific mechanical environment. The optimization method was applied to a high tibial osteotomy.

METHODS

Optimization Scheme

The scheme was based on two criteria: (i) the maximization of the relative amount of fluid exchanged between the bone substitute and its environment during one loading cycle, and (ii) the optimization of average fluid-induced shear stress amplitude $|\tilde{\tau}|$ at the interface between the fluid and the substitute to range between 0.03 and 3 Pa.

The first criterion was formulated as (see Appendix 1)

$$\max(\delta V^f) = \max\left[\frac{1}{\rho_0^f V_0^f}\int_t^{t+T}\int_\Gamma |\mathbf{q}^r\cdot\mathbf{n}|d\Gamma\, d\tilde{t}\right] \qquad (1)$$

where ρ_0^f is the initial fluid mass density, and V_0^f is the initial fluid volume inside the sample. The total fluid mass exchanged between the sample and its environment was determined by integration of the mass flux of fluid relative to the solid skeleton at the sample periphery $|\mathbf{q}^r\cdot\mathbf{n}|$ on the whole boundary Γ and on a time period T corresponding to one entire loading cycle.

The second criterion related to the average fluid-induced shear stress was expressed by (see Appendix 2)

$$0.03\cdot\mathrm{Pa} < \|\tilde{\tau}\| = \frac{\eta}{k\rho_0^f}\frac{\phi\phi_s}{\Sigma_{fs}}\|\mathbf{q}^r\| < 3\cdot\mathrm{Pa} \qquad (2)$$

Correspondence to: D.P. Pioletti (T: +41 21 693 83 41; F: +41 21 693 86 60; E-mail: dominique.pioletti@epfl.ch

where $\nu\ \gamma$ is the fluid viscosity, k is the sample isotropic permeability, ϕ_s and ϕ are the surface and volume porosities, and Σ_{fs} denotes the specific contact surface between the fluid and the solid.

The fluid mass flux $\mathbf{q}^r$ was assumed to be due to convective flux triggered by the deformation of the solid skeleton under dynamic mechanical loads. An explicit expression of the fluid mass flux time evolution and special distribution $\mathbf{q}^r(r,t)$ was obtained analytically for a simplified configuration (see Appendix 3). We considered a cylindrical porous sample of radius R and height h subjected to an oscillating dynamic compression force $F(t)$. The sample lower and upper boundaries were assumed impermeable and free flow condition was assumed at its periphery.

Application to Open Wedge Tibial Osteotomy

The relative fluid volume exchanged between the bone substitute and its environment and the fluid-induced shear stress were computed for the mechanical environment specific to high tibial osteotomy. The bone substitute target elastic modulus, Poisson's ratio, porosity, and permeability values were determined for three bone substitute geometries (Fig. 1) using the optimization criteria (Equations 1 and 2).

The mechanical environment of the bone substitute was determined using an existing finite element model.[36] Briefly, the tibial geometry and density distribution of a 35-year-old male were extracted from CT images. Transisotropic inhomogeneous properties were assumed. The osteotomy was performed on the computer under the supervision of a senior orthopedic surgeon, and homogeneous poroelastics bone substitutes of different sizes with different elastic modulus, porosity, permeability, and fluid viscosity values were placed in the tibial opening. A stainless steel supporting plate was screwed on both sides of the osteotomy by four screws proximally and two screws distally. Tibiofemoral contact forces corresponding to a gait cycle (Fig. 2) were applied to the tibia. The fluid mass flux inside the bone substitute due to its transient deformation was computed with a commercial finite element code Abaqus (Dassault Systèmes, France).

RESULTS

The analytical solution of Biot's poroelastic equations showed that fluid volume exchange between the bone substitute and its environment was inversely proportional to its elastic modulus, was proportional to $1-2\gamma$ ($\mu\mu$), and decreased with increasing porosity. The proportion of fluid exchange did not depend on fluid viscosity and porous media permeability. In other words, soft and compressible porous material exchanges more fluid per loading cycle than stiff and macroscopically incompressible material.

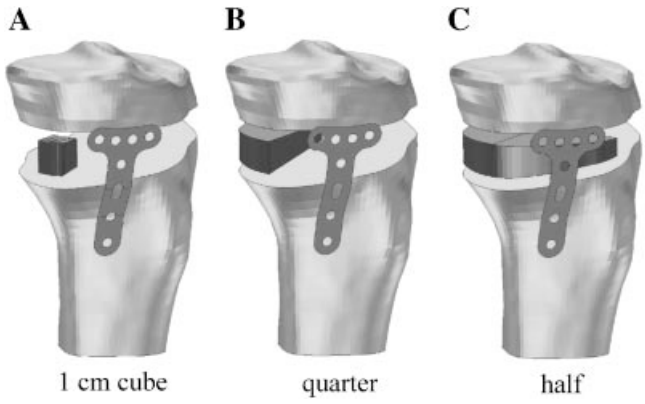

Figure 1. Finite element model of the open tibial osteotomy. Three bone substitute sizes were modeled: (A) a cube of 1 cm width, (B) a substitute covering one-quarter of the osteotomy cross sectional area, and (C) a substitute covering one-half of the osteotomy cross sectional area. Note that distances were increased between the elements for a better visualization.

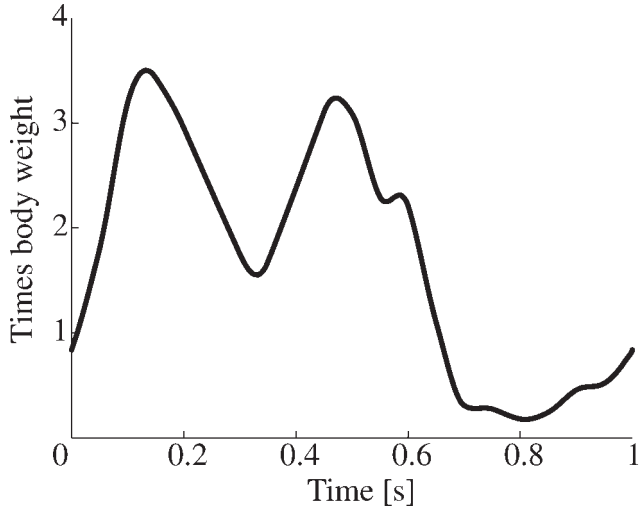

Figure 2. Tibiofemoral force during one gait cycle.[53]

The fluid-induced shear stress was inversely proportional to the bone substitute elastic modulus and permeability, and proportional to the fluid viscosity and to $1-2\gamma$ ($\mu\mu$). On the other hand, the porosity had no impact on the fluid-induced shear stress.

Optimization Scheme

The optimization of the fluid motion inside the bone substitute could be carried out in two steps (Fig. 3). First, the fluid volume exchange could be maximized by choosing the smallest possible elastic modulus, Poisson's ratio, and porosity. The minimization of these parameters should be carried out within an interval of values defined by other biomechanical aspects such as structural, technological, and biological requirements. Interestingly, this first step could be carried out independently of the load magnitude applied to the bone substitute. Second, the substitute permeability should be chosen so that the fluid-induced shear stress magnitude ranges between 0.03 and 3 Pa. This second step should take into account the variation of bone marrow viscosity that ranges between 0.05 and 0.6 $Pa \cdot s$.[37] However, the optimal permeability value obtained by the optimization scheme could lead to unrealistically high values. In this case, the target elastic modulus and Poisson's ratio could be increased until a realistic permeability value is obtained.

Application to High Tibial Osteotomy

The maximal compression stress at the bone substitute-bone interface during gait was 16 MPa for the 1 cm edge,

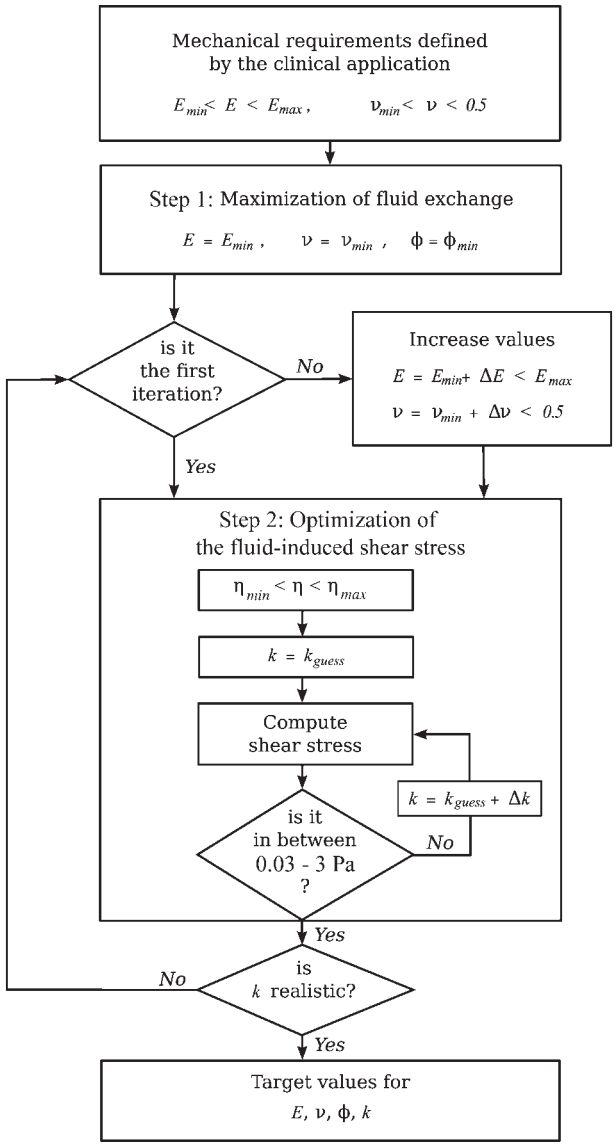

Figure 3. Flowchart to determine target mechanical and fluid conductivity properties of bone substitutes that optimize internal fluid flow.

cubic bone substitute (Fig. 1A), 3.3 MPa for the quarter one (Fig. 1B), and 1.8 MPa for the half one (Fig. 1C). To ensure structural stability of the osteotomy, the bone substitute elastic modulus should be >500 MPa. In addition, the range of Poisson's ratio was limited between 0.1 and 0.5 as material with zero or negative Poisson's ratio is difficult to achieve and requires specific processing procedures.[38,39] Finally, the range of porosity values was limited between 50 and 90% as good in vivo osteointegration was reported for various materials with these porosities.[4,14,40,41]

According to the optimization scheme, bone substitutes with elastic modulus of 500 MPa, Poisson's ratio of 0.1, and porosity of 50% are likely to maximize the proportion of fluid exchange. A 1 cm edge cubic bone substitute exchanged 10% of its fluid content with its environment during one gait cycle (Fig. 4), but the proportion fell to 5 and 0.5% when the elastic modulus

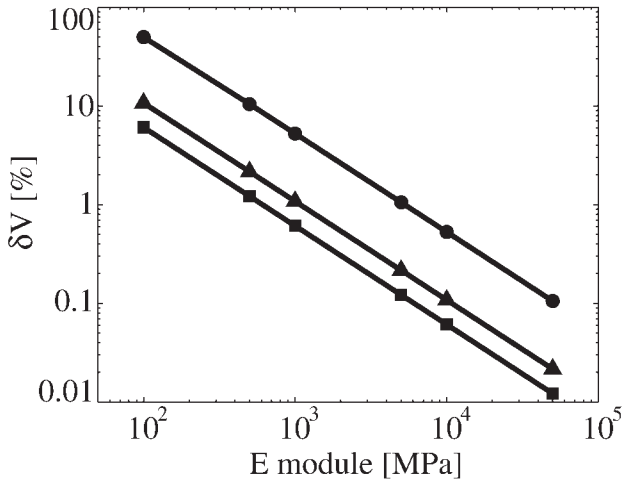

Figure 4. Proportion of fluid volume exchanged between the substitute and its environment during one gait cycle for three geometries: ●, 1 cm edge cube; ▲, one-quarter wedge; ■, one-half wedge.

was increased to 1 and 10 GPa, respectively. Decreasing the porosity from 75 to 50% increased the fluid volume exchange by 52% at constant elastic modulus (500 MPa). Decreasing the Poisson's ratio from 0.3 to 0.1 doubled the proportion of fluid exchange.

The maximum shear stress induced by fluid motion during gait inside a 1 cm edge cubic bone substitute was 58 Pa for an elastic modulus of 500 MPa and permeability of 6×10^{-11} m^2 (Fig. 5). The maximum target fluid-induced shear stress of 3 Pa was reached for materials with similar elastic moduli but with a permeability of 1.2×10^{-9} m^2, which is a realistic value.

Because large bone substitutes are subjected to lower compression stresses than smaller ones, the proportions of fluid exchange at equal elastic modulus (500 MPa) were 4.5-fold (2.2%) and ninefold (1.1%) smaller for quarter and for half bone substitutes than for a 1 cm edge cubic size. The smaller substitutes also exhibited

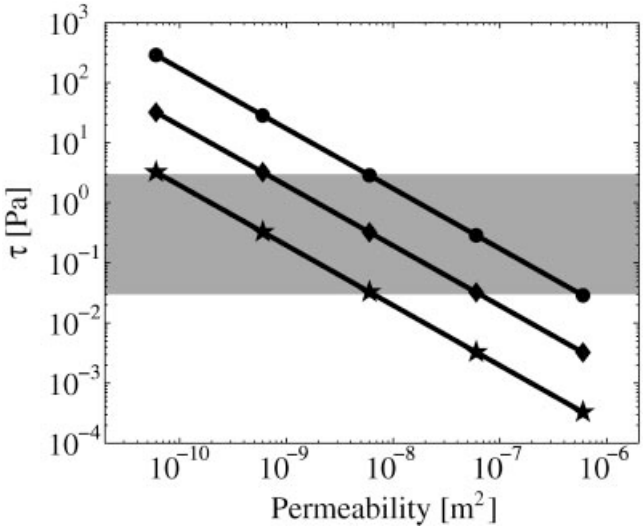

Figure 5. Fluid-induced shear stress in a 1 cm edge bone substitute as a function of its intrinsic permeability and for three elastic moduli: ●, $E = 100$ MPa; ◆, E = 1 GPa; ★, E = 10 GPa.

maximum fluid-induced shear stresses that were 1.7- and 2.0-fold smaller than those with a 1 cm edge cubic substitute with the same properties.

DISCUSSION

A growing corpus of evidence shows that fluid motion plays a central role in bone physiology and bone substitute osteointegration.[15–19] Fluid motion ensures the transport of nutriments, wastes, biochemical signals, and cells, and exerts a direct mechanical stimulation on bone cells. A balance between maximum fluid transport and fluid-induced shear stress should be achieved to favor osteointegration of a bone substitute. Our aim was to develop a method to identify bone substitute target elastic modulus, Poisson's ratio, porosity, and permeability to enhance fluid transport between the substitute and its environment while maintaining fluid-induced shear stress within a range that triggers osteogenesis.

In this study, we showed that materials with minimum elastic moduli, Poisson's ratios, and porosities likely enhance fluid transport within the substitute and with its environment. Structural, technological, and biological requirements, however, limit the choice of these physical parameters. For the particular case of high tibial osteotomy, a minimum elastic modulus of 500 MPa was needed for structural stability of the tibial plateau during gait, a minimum Poisson's ratio of 0.1 was assumed to avoid specific processing procedures,[38,39] and a minimum porosity of 50% was required to ensure good osteointegration.[4,14,40] As a result, high tibial osteotomy using a bone substitute material with these properties is likely to maximize fluid flow and favor rapid osteointegration. A bone substitute covering one-quarter of the osteotomy cross section exchanged 2.2% of its fluid content during each gait cycle for an optimized material compared to 0.6 and 0.4% for a substitute made of cancellous bone or coralline hydroxylapatite.

Interestingly, permeability had no impact on the proportion of fluid exchange, at least for values in the range of those measured for cancellous bone, coralline hydroxylapatite, porous tricalcium phosphate, and poly-L-lactide acide foam used for bone substitute.[39,41–45] Conversely, permeability had an inversely proportional impact on fluid-induced shear stress. Thus, the average mechanical stimulation applied to pre- and mature osteoblasts that colonize the bone substitute can be tuned by changing the permeability. For a 1 cm edge length cubic bone substitute used in high tibial osteotomy, a permeability of 1.2×10^{-9} m^2 will likely produce an average fluid-induced shear stress $\leq$3 Pa. Similarly, a substitute that covers one-quarter or one-half of the osteotomy cross section should present permeabilities of 7×10^{-10} and 6×10^{-10} m^2, respectively. Such values are comparable to those measured on cancellous bone,[42,43] but are two orders of magnitude larger than those measured for coralline hydroxylapatite[44] and porous poly-L-lactide acid foam.[46] Thus, the mechanical stress due to fluid motion inside these artificial bone substitutes used in high tibial osteotomy will likely damage cells and lead to poor osteointegration.

The main limitation of our study was a lack of experimental data to validate the theoretical elastic modulus, Poisson's ratio, porosity, and permeability values. However, the proposed optimization scheme is based on two strong pieces of experimental evidence that fluid transport and fluid-induced shear stress favor osteogenesis and osteointegration.[15–20] In addition, a theoretical approach seems more suited to assess the impact of various parameters and their possible interdependence than an empirical approach.

Although Biot's poroelastic theory neglects diffusion and dispersion, is linear elastic, and is based on Darcy's law, it has been successfully applied to bone mechanics.[15,47–49] Its extension to nonlinear materials and a more sophisticated conduction law is possible, but beyond the scope of this study.

In conclusion, fluid motion can be optimized by first minimizing the bone substitute elastic modulus, Poisson's ratio, and porosity within a predefined range of values given by structural, technological, and biological requirements. In a second step, the stimulation of bone cells by the fluid motion is optimized by tuning the bone substitute permeability. For high tibial osteotomy with a one-quarter wedge, the optimal fluid motion within the substitute is achieved by a material with an elastic modulus of 500 MPa, a Poisson's ratio of 0.1, a porosity of 50%, and permeability value of 7×10^{-10} m^2.

ACKNOWLEDGMENTS

This research was supported by the Swiss National Science Foundation (FNRS No. 2100-066872.01/1 and No. 205320-113408), the Fondation Lémanique pour la Recherche sur le Tissu Osseux, and the Lausanne Center for Bone Tissue Engineering.

Appendix 1

The total volume of fluid exchanged between the bone substitute domain Γ and its environment can be determined from the spatial and temporal distribution of the fluid mass flux $\mathbf{q}^r(\Gamma,t)$ relative to the bone substitute solid skeleton (see Appendix 3 for the calculation of $\mathbf{q}^r$). For every time t, the mass flux of fluid that crosses the bone substitute boundary $\partial\Gamma$ is given by the scalar product of the fluid mass flux $\mathbf{q}^r$ and the boundary normal $\mathbf{n}$:

$$\dot{m} = \int_{\partial\Gamma} |\mathbf{q}^r \cdot \mathbf{n}| \tag{1}$$

The total fluid volume exchanged during one oscillating period T is determined by integration of the instantaneous mass flux $\dot{m}$ over the time period:

$$m_{tot} = \int_t^{t+T} \dot{m} d\tilde{t} \tag{2}$$

Combining Eqns. (1) and (2) and normalizing by the initial fluid mass gives the proportion of fluid volume exchanged between the bone substitute and its environment.

Appendix 2

The average shear stress exerted by a moving fluid on the solid skeleton of a bone substitute was determined using the averaging theory applied to poroelastic media[50]. The average viscous drag at the solid-fluid interface $\bar{\tau}$ was obtained by averaging the microscopic mass balance

$$\bar{\tau} = -\frac{\eta}{\rho_0}\frac{\phi C_f}{\Delta_f^2 \Sigma_{fs}}\alpha \mathbf{q}^{\mathrm{r}} \tag{3}$$

In the above equation, the average shear stress is a function of the fluid viscosity η, the porosity ϕ, the macroscopic shape factor C_f, the fluid initial mass density ρ_0, the hydraulic radius Δ_f, the specific solid-fluid area Σ_{fs}, the solid-fluid interface shape matrix α, and the fluid mass flux relative to the solid skeleton $\mathbf{q}^{\mathrm{r}}$. Further deriving the Darcy's law for isotropic porous material gives the relation between the permeability k and the parameters appearing in Eqn. (3):

$$k = \frac{\phi^s \Delta_f^2}{C_f}\alpha^{-1} \tag{4}$$

where ϕ_s is the surface porosity. Substituting Eqn. (4) in Eqn. (3) gives the expression of the average drag force taking place at the solid-fluid interface:

$$\bar{\tau} = -\frac{\eta}{k\rho_0^f}\frac{\phi\phi^{\mathrm{s}}}{\Sigma_{fs}}\mathbf{q}^{\mathrm{r}} \tag{5}$$

Appendix 3

The solid skeleton equation of motion of a fully saturated, linear poroelastic material is given by:[51,52]

$$\frac{E}{2(1+\nu)(1-2\upsilon)}\nabla(\nabla\cdot\mathbf{u}) - \frac{E}{2(1+\nu)}\nabla^2\mathbf{u} + b\nabla p = 0 \tag{6}$$

where E and γ ($\mu\mu$) are the drained elastic modulus and Poisson's ratio, respectively, $\mathbf{u}$ is the solid skeleton, and b is the Biot's coefficient. The fluid equation of motion is given by:

$$\frac{\eta}{kM}\frac{\partial p}{\partial t} + \frac{\eta b}{k}\frac{\partial}{\partial t}\nabla\cdot\mathbf{u} - \nabla^2 p = 0 \tag{7}$$

where M is the Biot's modulus. The coupled system of differential equations (6 and 7) can be solved analytically for an axisymmetric sample, assuming solid deformation of the form $\mathbf{u} = u(r,t)\mathbf{e}_r + w(z,t)\mathbf{e}_z$. The upper and lower cylinder boundaries are considered impermeable, and a constant pressure p_0 is assumed at the cylinder outer boundary. The pressure distribution inside the cylindrical sample when submitted to a cyclic compression axial force $F(t)$ is thus:

$$p(r,t) - p_0 = \sum_{n=1}^{\infty} p_n(t) J_0(k_n r) \tag{8}$$

where $p_n(t)$ is the pressure time evolution, and J_0 is the J-Bessel function of order 0. Finally, Darcy's law yields to the expression for the fluid mass flux relative to the solid skeleton:

$$q^r(r,t)\mathbf{e}_r = \frac{k}{\eta\phi}\sum_{n=1}^{\infty} p_n(t)\frac{J_1(k_n r)}{k_n}\mathbf{e}_r \tag{9}$$

REFERENCES

1. Bohner M, van Lenthe GH, Grunenfelder S, et al. 2005. Synthesis and characterization of porous beta-tricalcium phosphate blocks. Biomaterials 26:6099–6105.
2. Taboas JM, Maddox RD, Krebsbach PH, et al. 2003. Indirect solid free form fabrication of local and global porous, biomimetic and composite 3D polymer-ceramic scaffolds. Biomaterials 24:181–194.
3. Doernberg MCV, Rechenberg BV, Bohner M, et al. 2006. In vivo behavior of calcium phosphate scaffolds with four different pore sizes. Biomaterials 27:5186–5198.
4. Fisher JP, Vehof JW, Dean D, et al. 2002. Soft and hard tissue response to photocrosslinked poly(propylene fumarate) scaffolds in a rabbit model. J Biomed Mater Res 59:547–556.
5. Chang BS, Lee CK, Hong KS, et al. 2000. Osteoconduction at porous hydroxyapatite with various pore configurations. Biomaterials 21:1291–1298.
6. Uchida A, Nade SM, McCartney ER, et al. 1984. The use of ceramics for bone replacement. A. comparative study of three different porous ceramics. J Bone Joint Surg 66:269–275.
7. Flautre B, Descamps M, Delecourt C, et al. 2001. Porous HA ceramic for bone replacement: role of the pores and interconnections—experimental study in the rabbit. J Mater Sci 12:679–682.
8. Lu JX, Flautre B, Anselme K, et al. 1999. Role of interconnections in porous bioceramics on bone recolonization in vitro and in vivo. J Mater Sci Mater Med 10:111–120.
9. Gauthier O, Bouler JM, Aguado E, et al. 1998. Macroporous biphasic calcium phosphate ceramics: influence of macropore diameter and macroporosity percentage on bone ingrowth. Biomaterials 19:133–139.
10. Kuhne JH, Bartl R, Frisch B, et al. 1994. Bone formation in coralline hydroxyapatite. Effects of pore size studied in rabbits. Acta Ortho Scan 65:246–252.
11. Hulbert SF, Morrison SJ, Klawitter JJ. 1972. Tissue reaction to three ceramics of porous and non-porous structures. J Biomed Mater Res 6:347–374.
12. Eggli PS, Muller W, Schenk RK. 1988. Porous hydroxyapatite and tricalcium phosphate cylinders with two different pore size ranges implanted in the cancellous bone of rabbits. A. comparative histomorphometric and histologic study of bony ingrowth and implant substitution. Clin Orthop Rel Res 232:127–232.
13. Itala AI, Ylanen HO, Ekholm C, et al. 2001. Pore diameter of more than 100 micron is not requisite for bone ingrowth in rabbits. J Biomed Mater Res 58:679–683.
14. Karageorgiou V, Kaplan D. 2005. Porosity of 3D biomaterial scaffolds and osteogenesis. Biomaterials 26:5474–5491.
15. Prendergast PJ, Huiskes R, Soballe K. 1997. ESB research award1996.biophysical stimuli on cells during tissue differentiation at implant interfaces. J Biomech 30:539–548.
16. Sikavitsas VI, Temenoff JS, Mikos AG. 2001. Biomaterials and bone mechanotransduction. Biomaterials 22:2581–2593.

17. Turner CH, Robling AG. 2004. Mechanical loading and bone formation. BoneKEy-Osteovision 1:15–23.
18. Hui PW, Leung PC, Sher A. 1996. Fluid conductance of cancellous bone graft as a predictor for graft-host interface healing. J Biomech 29:123–132.
19. Thi MM, Iacobas DA, Iacobas S, et al. 2007. Fluid shear stress upregulates vascular endothelial growth factor gene expression in osteoblasts. Ann NY Acad Sci 1117:73–81.
20. Goldstein AS, Juarez TM, Helmke CD, et al. 2001. Effect of convection on osteoblastic cell growth and function in biodegradable polymer foam scaffolds. Biomaterials 22: 1279–1288.
21. Tate MLK, Knothe U. 2000. An ex vivo model to study transport processes and fluid flow in loaded bone. J Biomech 33:247–254.
22. Sikavitsas VI, Bancroft GN, Holtorf HL, et al. 2003. Mineralized matrix deposition by marrow stromal osteoblasts in 3D perfusion culture increases with increasing fluid shear forces. Proc Natl Acad Sci USA 100:14683–14688.
23. Barbee KA. 2005. Mechanical cell injury. Ann NY Acad Sci 1066:67–84.
24. Jiang GL, White CR, Stevens HY, et al. 2002. Temporal gradients in shear stimulate osteoblastic proliferation via ERK1/2 and retinoblastoma protein. Am J Physiol Endocrinol Metab 283:E383–E389.
25. Mullender MG, Dijcks SJ, Bacabac RG, et al. 2006. Release of nitric oxide, but not prostaglandin E2, by bone cells depends on fluid flow frequency. J Orthop Res 24:1170–1177.
26. Burger EH, Nulend JK. 1999. Mechanotransduction in bone—role of the lacuno-canalicular network. FASEB J 13:S101–S112.
27. Nulend JK, Burger EH, Semeins CM, et al. 1997. Pulsating fluid flow stimulates prostaglandin release and inducible prostaglandin G/H synthase mRNA expression in primary mouse bone cells. J Bone Miner Res 12:45–51.
28. Litzenberger JB, Tummala P, Jacobs CR. 2006. Integrin signaling and the response of osteocytes to oscillatory fluid flow. MCB Mol Cell Biomech 3:219–220.
29. Kapur S, Baylink DJ, Lau KHW. 2003. Fluid flow shear stress stimulates human osteoblast proliferation and differentiation through multiple interacting and competing signal transduction pathways. Bone 32:241–251.
30. You J, Yellowley CE, Donahue HJ, et al. 2000. Substrate deformation levels associated with routine physical activity are less stimulatory to bone cells relative to loading-induced oscillatory fluid flow. J Biomech Eng 122:387–393.
31. Wadhwa S, Choudhary S, Voznesensky M, et al. 2002. Fluid flow induces COX-2 expression in MC3T3M-E1 osteoblasts via a PKA signaling pathway. Biochem Biophys Res Commun 297:46–51.
32. Tanaka SM, Li J, Duncan RL, et al. 2003. Effects of broad frequency vibration on cultured osteoblasts. J Biomech 36:73–80.
33. Tanaka SM, Sun HB, Roeder RK, et al. 2005. Osteoblast responses one hour after load-induced fluid flow in a three-dimensional porous matrix. Calcif Tissue Int 76:261–271.
34. Ignatius A, Blessing H, Liedert A, et al. 2005. Tissue engineering of bone: effects of mechanical strain on osteoblastic cells in type I collagen matrices. Biomaterials 26:311–318.
35. Blackman BR, Barbee KA, Thibault LE. 2000. In vitro cell shearing device to investigate the dynamic response of cells in a controlled hydrodynamic environment. Ann Biomed Eng 28:363–372.
36. Blecha LD, Zambelli PY, Ramaniraka NA, et al. 2005. How plate positioning impacts the biomechanics of the open wedge tibial osteotomy; A finite element analysis. Comput Meth Biomech Biomed Eng 8:307–313.
37. Bryant JD, David T, Gaskell PH, et al. 1989. Rheology of bovine bone marrow. Proc Inst Mech Eng H J Eng Med 203:71–75.
38. Friis EA, Lakes RS, Park JB. 1988. Negative {P}oisson's ratio polymeric and metallic foams. J Mater Sci 23:4406–4414.
39. Gibson LJ, Ashby MF. 1997. Cellular solids—Structure and properties. Cambridge: Cambridge University Press.
40. Kujala S, Ryhanen J, Danilov A, et al. 2003. Effect of porosity on the osteointegration and bone ingrowth of a weight-bearing nickel-titanium bone graft substitute. Biomaterials 24:4691–4697.
41. Zhang C, Wang J, Feng H, et al. 2001. Replacement of segmental bone defects using porous bioceramic cylinders: a biomechanical and X-ray diffraction study. J Biomed Mater Res 54:407–411.
42. Nauman EA, Fong KE, Keaveny TM. 1999. Dependence of intertrabecular permeability on flow direction and anatomic site. Ann Biomed Eng 27:517–524.
43. Rice JC, Cowin SC, Bowman JA. 1988. On the dependence of the elasticity and strength of cancellous bone on apparent density. J Biomech 21:155–168.
44. Haddock SM, Debes JC, Nauman EA, et al. 1999. Structure-function relationships for coralline hydroxyapatite bone substitute. J Biomed Mater Res 47:71–78.
45. Gibson LJ, Ashby MF. 1982. The mechanics of three-dimensional cellular materials. Proc Royal Soc Lond Ser A: Math Phys Sci 382:43–59.
46. Blecha LD. 2007. Theoretical and experimental multi-scale study of an artificial bone construct: from tibial osteotomy to cell-fluid interaction. Lausanne. Ecole Polytechnique Fédrale de Lausanne.
47. Cowin SC. 1999. Bone poroelasticity. J Biomech 32:217–238.
48. Kohles SS, Roberts JB. 2002. Linear poroelastic cancellous bone anisotropy: trabecular solid elastic and fluid transport properties. J Biomech Eng 124:521–526.
49. Swan CC, Lakes RS, Brand RA, et al. 2003. Micromechanically based poroelastic modeling of fluid flow in Haversian bone. J Biomech Eng 125:25–37.
50. Bear J, Bachmat Y. 1991. Introduction to modeling of transport phenomena in porous media. Dordrecht: Kluwer Academic Publishers.
51. Biot MA. 1941. General Theory of Three-Dimensional Consolidation. J Appl Phys 12:155–164.
52. Coussy O. 1991. Méchanique des milieux poreux. Paris: Editions Technip.
53. Taylor WR, Heller MO, Bergmann G, et al. 2004. Tibiofemoral loading during human gait and stair climbing. J Orthop Res 29:625–632.